

The X-ray spectrum of the bursting atoll source 4U 1728-34 observed with INTEGRAL

M. Falanga^{1,2,*}, D. Götz¹, P. Goldoni^{1,2}, R. Farinelli³, A. Goldwurm^{1,2}, S. Mereghetti⁴, A. Bazzano⁵,
L. Stella⁶

¹ CEA Saclay, DSM/DAPNIA/Service d'Astrophysique (CNRS FRE 2591), F-91191, Gif sur Yvette, France

² Unité mixte de recherche Astroparticule et Cosmologie, 11 place Berthelot, 75005 Paris, France

³ Dipartimento di Fisica, Università di Ferrara, via Paradiso 12, 44100 Ferrara, Italy

⁴ INAF-Istituto di Astrofisica Spaziale e Fisica Cosmica, Milano, via Bassini 15, 20133 Milano, Italy

⁵ INAF-Istituto di Astrofisica Spaziale e Fisica cosmica, via del Fosso del Cavaliere 100, 00133 Roma, Italy

⁶ INAF-Osservatorio Astronomico di Roma, via Frascati 33, 00040 Monteporzio Catone (Roma), Italy

the date of receipt and acceptance should be inserted later

Abstract. We present for the first time a study of the 3–200 keV broad band spectra of the bursting atoll source 4U 1728-34 (GX 354-0) along its hardness intensity diagram. The analysis was done using the *INTEGRAL* public and Galactic Center deep exposure data ranging from February 2003 to October 2004. The spectra are well described by a thermal Comptonization model with an electron temperature from 35 keV to 3 keV and Thomson optical depth, τ_T , from 0.5 to 5 in a slab geometry. The source undergoes a transition from an intermediate/hard to a soft state where the source luminosity increases from 2 to 12% of Eddington. We have also detected 36 type I X-ray bursts two of which show photospheric radius expansion. The energetic bursts with photospheric radius expansion occurred at an inferred low mass accretion rate per unit area of $\dot{m} \sim 1.7 \times 10^3 \text{ g cm}^{-2} \text{ s}^{-1}$, while the others at a higher one between $2.4 \times 10^3 - 9.4 \times 10^3 \text{ g cm}^{-2} \text{ s}^{-1}$. For 4U 1728-34 the bursts' total fluence, and the bursts' peak flux are anti-correlated with the mass accretion rate. The type I X-ray bursts involve pure helium burning either during the hard state, or during the soft state of the source.

Key words. binaries: close – stars: individual (4U 1728-34) – stars: neutron – X-rays: bursts

1. Introduction

Low-mass X-ray binary systems (LMXBs), consisting of an accreting neutron star (NS) and a main-sequence donor star ($M < 1 M_\odot$), are usually classified as atoll or Z sources, according to the path they describe in an X-ray colour-colour diagram (CCD) or hardness-intensity diagram (HID). The main difference between atoll and Z sources is in the accretion rate, the magnetic field and probably in the spin rate and the geometry of the system. For atoll sources, the positions along the characteristic branches have historically been called the “island”, “lower banana” and “upper banana” branches, which indicate the spectral states probably as a function of the mass accretion rate (Hasinger & van der Klis, 1989). The mass accretion rate increases from the island state (hard spectral states) where the soft emission is much reduced and the spectrum is dominated at high energies up to 200 keV, to the banana states (soft spectral states) where most of

the energy is emitted below ~ 20 keV (e.g., Barret, 2001; Gierliński & Done, 2002).

The atoll sources show luminosities smaller than those of Z sources (generally less than 10 per cent of Eddington, L_{Edd}), low magnetic fields ($B \sim 10^8 \text{ G}$), and spectral variability, or equivalently, motion along the banana branch over a timescale of hours to days, and more slowly in the island state from days to weeks.

Some atoll sources also show time variability properties in their power spectra, such as Quasi-Periodic Oscillations (QPOs), which are strongly correlated with the position on the CCD/HID (Hasinger & van der Klis, 1989). Almost all the timing features characterizing the power density spectra of these sources seem to vary in a smooth and monotonic way when the source moves along its CCD/HID (Wijnands & van der Klis, 1999; Psaltis, Belloni & van der Klis, 1999), implying a tight correlation between spectral and temporal behaviour (for a review see van der Klis, 2004). In most atoll sources, QPOs are observed in the frequency range from millihertz to the kilohertz. Kilohertz QPOs or twin kHz QPOs in the frequency range from 300–1200 Hz are usually observed in

Send offprint requests to: M. Falanga

* e-mail: mfalanga@cea.fr

the island state and lower banana branch (van der Klis, 2004, and references therein).

In some of the atoll sources, type I X-ray bursts are also observed (e.g., Lewin & Joss, 1983). Type I X-ray bursts are characterized by a fast rise and exponential decay with durations ranging from seconds to tens of minutes. These bursts are due to unstable hydrogen/helium burning in a thin shell on the NS surface (see e.g., the review by Lewin, van Paradjis, & Taam, 1993). The burst spectrum can be described by blackbody radiation with cooling during the decay of the burst. The gradual decay persists longer at lower energies, indicating that the burst spectrum is characterized by steadily decreasing blackbody temperatures (e.g., Lewin & Joss, 1983). During these bursts nearly-coherent oscillations are sometimes observed, the frequencies of which are in the rather narrow range between 300 and 600 Hz (Strohmayer & Markwardt, 1999; Strohmayer & Bildsten, 2004). This frequency is interpreted as the NS rotation frequency due to a hot spot (or spots) in an atmospheric layer of the rotating NS (Chakrabarty et al., 2003).

The CCDs diagrams and HIDs are powerful ways of parameterizing the spectral changes using physically motivated spectral models to understand the underlying physical changes in the source emission. In this work, we study for the first time the broad band (3-200 keV) spectral shape of the atoll source 4U 1728-34 as a function of its HID position. The correlation of type I X-ray burst properties with source state in the HID is also investigated. We analyze the *International Gamma-Ray Astrophysics Laboratory (INTEGRAL)* 2003/2005 data concentrating also on the high energy emission of 4U 1728-34. This paper deals only with type I X-ray bursts, therefore whenever we write burst(s), we mean type I X-ray burst(s).

1.1. The source 4U 1728-34

The persistent LMXB source 4U 1728-34 (or GX 354-0) is a well known burster discovered by Uhuru and classified as an atoll source from its colour-colour diagram and timing properties (Forman, Tananbaum & Jones, 1976; Hoffman et al., 1976; Hasinger & van der Klis, 1989). However, little is known about the system as the optical counterpart is not identified due to the high optical extinction in the direction of the Galactic center. The distance is poorly known, the current estimate being between 4.4–5.1 kpc using photospheric radius expansion burst luminosity as a standard candle (Di Salvo et al., 2000; Galloway et al., 2003). This is based on the assumption that the bolometric burst peak luminosity during photospheric radius expansion is saturated at the Eddington limit.

The time averaged persistent soft (0.1 keV) to hard (300 keV) X-ray emission spectrum of 4U 1728-34 was studied in the past using *Einstein*, *SAS 3*, *EXOSAT SIGMA* and *ROSAT* data (Grindlay & Hertz,

1981; Basinska et al., 1984; White et al., 1986; Claret et al., 1994; Schulz, 1999) and, more recently, using *RXTE*, *BeppoSAX*, *ASCA* and *Chandra* (Di Salvo et al., 2000; Piraino, Santangelo & Kaaret, 2000; Narita, Grindlay & Barret, 2001; D’Ai et al., 2006). The spectrum was well fitted by a thermal bremsstrahlung or thermal Comptonization model as well as a Gaussian emission line at the energy ~ 6.7 keV. Different spectral parameters were found for the electron temperature and Thomson optical depth, which can be explained by the varying state of the source in its CCD/HID position.

During all spectral states, bursts of ~ 10 – 20 s duration were observed (e.g., Cornelisse et al., 2003). The burst spectrum can be fitted by a blackbody with temperature increasing from 1 to 3 keV during the burst rise time. Most of these bursts show evidence for photospheric radius expansion (Hoffman et al., 1976; White et al., 1986; Day & Tawara, 1990; Foster, Ross, & Fabian, 1986; Franco, 2001; van Straaten, 2001; Galloway et al., 2003, 2006). Flux oscillations at 363 Hz during the bursts were discovered in this source with the *Rossi X-ray Timing Explorer (RXTE)*, and interpreted as the spin frequency of the NS (Strohmayer et al., 1996; Chakrabarty et al., 2003). Apart from the bursting activity, 4U 1728-34 also exhibits complex behaviour on short time scale. It was also the first neutron star LMXB to show twin kHz QPOs in the persistent emission with a frequency separation almost constant at ~ 350 Hz (e.g., Méndez & van der Klis, 1999; Di Salvo et al., 2001; Migliari, van der Klis, & Fender, 2003, and references therein).

2. Observations and Data

The present data set was obtained with the *INTEGRAL* observatory (Winkler et al., 2003) using the 2003/2005 Core Program Galactic Center Deep Exposure observations and publicly available data. We analyzed data from the Imager on Board the Integral Satellite (IBIS) coded mask INTEGRAL Soft Gamma-Ray Imager (ISGRI) (Ubertini et al., 2003; Lebrun et al., 2003) at energies between 20 and 200 keV and from the JEM-X monitor, module 1 and 2 (Lund et al., 2003) between 3 and 20 keV. For ISGRI and JEM-X, the data were extracted for all pointings within $\leq 3^\circ 5$ from the source direction. The available data consist of 356 individual pointings for a total effective exposure of 640 ks. Data reduction was performed using the standard Offline Science Analysis (OSA) software version 5.0 distributed by the *INTEGRAL* Science Data Centre (ISDC) (Courvoisier et al., 2003). The algorithms used in the IBIS/ISGRI analysis are described in Goldwurm et al. (2003).

The brightest bursts were detected using the *INTEGRAL* Burst Alert System (IBAS) software (Mereghetti et al., 2003) running at ISDC. IBAS is dedicated to the real time discovery and localization of gamma-ray bursts, transient X-ray sources and bursts

in the IBIS/ISGRI data stream. Bursts are identified by scanning the data binned using different timescales (from a few milliseconds to 100 s) and energy ranges. One of IBAS operation modes, running on the 15–40 keV energy interval and 10 s time scale, is particularly suited to detect type I X-ray bursts. Typically the bursts are localized with a $\sim 3'$ uncertainty. The fainter bursts were detected using 2 s rebinned JEM-X light curves in the 3–20 keV energy band. Most of the bursts detected with JEM-X were also detected with ISGRI in the 18–40 keV energy band, these flux excesses were confirmed also by the imaging as related to the source position. So, we call the bursts detected with IBAS “bright bursts” and the ones detected only with JEM-X “weak bursts”.

The burst light curves are based on events selected according to the detector illumination pattern for 4U 1728-34; for ISGRI we used an illumination threshold of 0.6 for the energy range 18–40 keV. For JEM-X we used the event list of the whole detector in the 3–6 keV, 6–12 keV and 12–20 keV energy band. In Table 1 we report the burst start time detected with *INTEGRAL* from February 2003 to January 2005. The start time for each burst was determined when the intensity was 10% of the peak above the persistent intensity level. Note that six of the IBAS detected bursts were outside of the JEM-X field of view. Due to the lack of the low energy data we excluded these bursts from the analysis. However we report the burst start times and durations (see Table 1).

3. Results

To study the light curves and spectra of 4U 1728-34 we first deconvolved and analyzed separately the 356 pointings and then combined them into a total mosaic image in the 20–40 keV energy band. In the mosaic 4U 1728-34 is clearly detected, as well as the nearby source the Rapid Burster (4U 1730-335). The source position offsets with respect to the catalog positions are $0'.2$ for 4U 1728-34 and $0'.23$ for the Rapid Burster. This is within the 90% confidence level assuming the source location error given by Gros et al. (2003). The derived angular distance between the two sources is $\sim 31'.5$. Due to the fact that *INTEGRAL* is able to image the sky at high angular resolution ($12'$ for ISGRI and $3'$ for JEM-X), we were able to clearly distinguish and isolate the high-energy fluxes from the two sources. This allowed us to study the X-ray emission of 4U 1728-34 during its entire observation without contamination (see also for the Rapid Burster Falanga et al., 2004). In Fig. 1 we show the JEM-X (top) 3–20 keV and ISGRI (bottom) 20–100 keV light curves extracted from all the 356 images. Pointings during which bursts were detected are marked in red (bright burst) and green (weak burst). The source is very active and strong variations on a short time scale are not uncommon. Bursts were observed during all intensity states. We also observed an isolated strong flare (around 53058 MJD), during which the source count rate increases from ~ 5 cts s^{-1} to ~ 50 cts s^{-1} in the soft energy band, 3–20 keV, and shows a

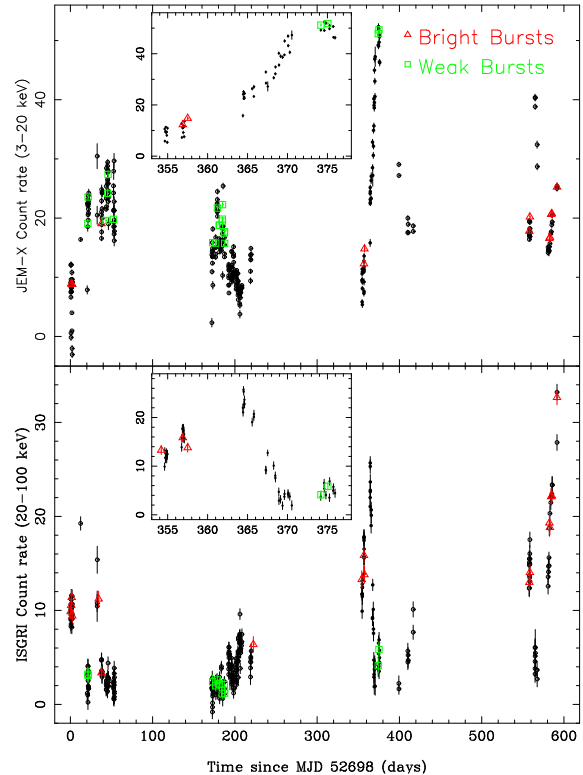


Fig. 1. JEM-X and IBIS/ISGRI light curves of 4U 1728-34 in the 3–20 keV and 20–100 keV energy bands. We indicate with red and green the net intensity (burst subtracted) emission where bursts were emitted. Each point corresponds to a pointing of ~ 1800 s duration. The 21-day flare is shown on a smaller time scale in the insets.

different trend at higher energy, 20–100 keV. During this flare, lasting ~ 21 days, the source undergoes a transition from a hard to a soft state (see Sect. 3.3). Note that during this flare two weak bursts happen at the peak of the 3–20 keV flux.

3.1. Burst light curves

In total, we observed 36 bursts, which we label numerically according to time. Their main properties are listed in Table 1. Based on JEM-X/ISGRI light curves in the 3–6 keV, 6–12 keV, 12–20 keV and 20–40 keV energy bands, rebinned at 0.5 s, we determined that the bursts have rise times of 1 ± 0.5 s. The decay time at 12–20 keV energy is significantly shorter than that in the 3–6 keV range, indicating spectral softening during each burst decay. This was also verified by determining hardness ratios, using the three JEM-X energy bands. For JEM-X the flux decays to quiescence with an mean exponential time-scale $F \propto e^{-t/4.5^s}$ (see Table 1). At high energy, the bursts were only significantly detected in the first $\Delta T_{\text{Burst}} \sim 5\text{--}10$ s (see Table 1). In Fig. 2 we show six JEM-X/ISGRI representative burst light curves in different energy bands. For bursts 2 and 4, a double peak profile is evident at high energy (lower panel) within the

Table 1. Log of *INTEGRAL* burst observations analyzed in this paper and spectral properties of the bursts.

Burst Nr.	IBIS/JEMX Date	IBIS/JEM-X T _{start} (UTC)	IBIS ΔT_{Burst}	JEMX		BURST E _b	PARAMETERS				
				τ_{exp}	\dot{m}		F _{peak}	τ	γ	α	
1 [†]	2003 Feb 28	07:55:01	8.4(3)	–	–	–	–	–	–	–	–
2 [†]	2003 Mar 01	00:04:45	8.2(3)	6.8(5)	1.7(2)	8.3(3)	9.6(3)	8.6(6)	0.012(4)	~ 110	–
3 [†]	2003 Mar 01	16:05:27	9.4(3)	–	–	–	–	–	–	–	–
4 [†]	2003 Mar 02	07:42:17	11.0(3)	6.8(5)	1.7(2)	8.9(3)	9.9(3)	9.0(4)	0.016(3)	~ 100	–
5	2003 Mar 21	06:09:48	5.7(3)	4.5(5)	3.2(2)	3.5(3)	3.9(3)	9.0(9)	0.07(7)	–	–
6	2003 Mar 21	15:46:38	3.5(3)	3.6(5)	4.3(2)	3.2(2)	7.9(2)	4.1(3)	0.051(2)	~ 270	–
7 [†]	2003 Apr 03	08:40:16	4.2(3)	–	–	–	–	–	–	–	–
8 [†]	2003 Apr 06	19:45:28	5.8(3)	5.9(5)	3.7(2)	5.1(4)	7.4(4)	6.9(6)	0.046(8)	–	–
9	2003 Apr 12	07:12:20	*	3.2(5)	3.5(2)	2.6(2)	4.4(2)	5.8(5)	0.073(6)	–	–
10	2003 Apr 14	09:05:15	*	3.4(5)	3.7(2)	1.9(2)	3.4(2)	5.5(7)	0.103(8)	–	–
11	2003 Apr 14	20:13:47	*	5.0(5)	4.5(3)	2.7(3)	3.8(2)	7.1(9)	0.111(8)	~ 610	–
12	2003 Apr 21	09:31:41	*	5.4(5)	3.7(2)	2.1(2)	3.6(2)	5.8(6)	0.062(7)	–	–
13	2003 Apr 19	22:57:35	3.5(3)	3.4(5)	2.7(2)	3.1(2)	5.1(2)	6.1(5)	0.049(4)	–	–
14	2003 Aug 23	16:14:00	4.2(3)	5.0(5)	2.7(2)	3.5(2)	6.1(2)	5.7(4)	0.042(4)	–	–
15	2003 Aug 25	18:24:08	6.0(3)	4.1(5)	3.9(2)	3.6(2)	6.6(2)	5.5(3)	0.056(3)	–	–
16	2003 Aug 28	01:23:58	7.6(3)	3.6(5)	3.2(5)	3.9(5)	5.5(5)	7.1(6)	0.055(5)	–	–
17	2003 Aug 28	06:01:29	4.6(3)	2.6(5)	3.3(5)	3.1(5)	5.3(5)	5.8(6)	0.057(6)	~ 160	–
18	2003 Aug 31	15:54:14	6.8(3)	6.5(5)	3.1(4)	3.1(4)	6.3(4)	5.0(7)	0.046(7)	–	–
19	2003 Aug 31	20:00:09	*	4.0(3)	3.5(3)	1.9(4)	3.9(4)	4.9(9)	0.08(1)	~ 240	–
20	2003 Aug 31	23:48:20	*	5.6(3)	4.6(2)	3.1(3)	3.7(3)	8.4(9)	0.12(1)	~ 200	–
21	2003 Sep 03	03:26:33	5.0(3)	3.1(5)	3.1(3)	3.8(5)	7.1(5)	5.3(8)	0.04(7)	–	–
22	2003 Sep 03	08:39:29	6.8(3)	4.9(5)	2.9(5)	2.8(3)	4.5(3)	6.2(7)	0.06(5)	~ 170	–
23	2003 Sep 03	13:07:21	2.7(3)	3.9(5)	2.8(4)	2.1(4)	4.4(4)	4.8(9)	0.06(1)	~ 220	–
24 [†]	2003 Oct 08	09:58:35	5.5(3)	–	–	–	–	–	–	–	–
25 [†]	2004 Feb 17	04:47:27	9.9(3)	–	–	–	–	–	–	–	–
26 [†]	2004 Feb 19	21:06:41	5.6(3)	1.97(5)	2.4(4)	4.2(4)	8.2(4)	5.1(5)	0.028(5)	–	–
27 [†]	2004 Feb 20	12:00:21	6.3(5)	–	–	–	–	–	–	–	–
28	2004 Mar 08	04:14:44	4.5(3)	5.2(5)	12.4(3)	3.3(3)	6.8(3)	4.8(6)	0.171(5)	–	–
29	2004 Mar 09	00:58:20	4.9(3)	3.6(5)	10.4(4)	3.5(4)	6.9(4)	5.0(7)	0.14(5)	~ 690	–
30	2004 Sep 07	21:30:45	5.0(3)	3.1(5)	3.8(3)	4.2(3)	7.0(3)	6.0(6)	0.056(5)	–	–
31 [†]	2004 Sep 08	12:44:37	6.8(3)	4.9(5)	4.1(3)	4.6(3)	7.3(3)	6.3(6)	0.052(5)	~ 450	–
32 [†]	2004 Oct 02	05:59:14	2.7(3)	3.9(5)	4.1(3)	4.1(3)	6.9(3)	5.9(6)	0.054(6)	–	–
33 [†]	2004 Oct 02	21:51:07	6.1(3)	5.5(5)	3.7(4)	3.6(4)	7.7(4)	4.7(5)	0.074(5)	~ 550	–
34 [†]	2004 Oct 04	12:29:37	4.5(3)	5.2(5)	4.7(3)	3.9(3)	7.3(3)	5.3(5)	0.059(6)	–	–
35 [†]	2004 Oct 05	05:59:09	6.0(3)	4.6(5)	5.5(3)	4.0(3)	6.7(3)	5.9(5)	0.082(5)	~ 780	–
36 [†]	2004 Oct 11	12:59:09	4.9(3)	6.8(5)	1.7(3)	3.5(3)	7.0(3)	5.0(5)	0.091(6)	–	–

Notes : [†] bright type I X-ray bursts. * not a statistically significant detection in ISGRI. The burst exponential decay time, τ_{exp} , is in units of seconds in the 3–20 keV energy band. The mass accretion rate per unit area of the persistent emission before the bursts, \dot{m} , are expressed in units of $10^3 \text{ g cm}^{-2} \text{ s}^{-1}$, assuming a canonical NS radius of 10 km. The net burst fluence, E_b , and the net peak flux, F_{peak} , (both persistent emission subtracted) are in units of $10^{-7} \text{ erg cm}^{-2}$ and $10^{-8} \text{ erg cm}^{-2} \text{ s}^{-1}$, respectively. The bursts parameters $\tau = E_b/F_{\text{peak}}$ is in units of seconds, and $\gamma = F_{\text{pers}}/F_{\text{peak}}$ is also listed for each burst. The quantity α is defined as the ratio of the total energy emitted in the persistent flux to that emitted in bursts, $\alpha = F_{\text{pers}}\Delta t/E_b$, where Δt is the time interval from the beginning of one burst to the next. We report only the most confident α values, i.e. without data gap between two burst.

first 10 s, while during this time the intensity at lower energy (upper panel) remains constant. This can be interpreted as a consequence of a photospheric radius expansion (PRE) episode during the first part of the outburst (see e.g., Verbunt & van den Heuvel, 1995). When a burst undergoes a PRE episode, due to radiation pressure, the luminosity, L , remains constant at the Eddington value, L_{Edd} , and, at high energy, a double peak profile can be observed. Such behaviour is well known for 4U 1728-34 and was observed previously in different bursts and recently

reported with *RXTE* data (Franco, 2001; van Straaten, 2001; Galloway et al., 2003, 2006).

We attempted to test the hypothesis of a PRE using the four different JEM-X/ISGRI energy bands and we measured such a double peak behaviour in the hardness ratio only for burst 2 and 4.

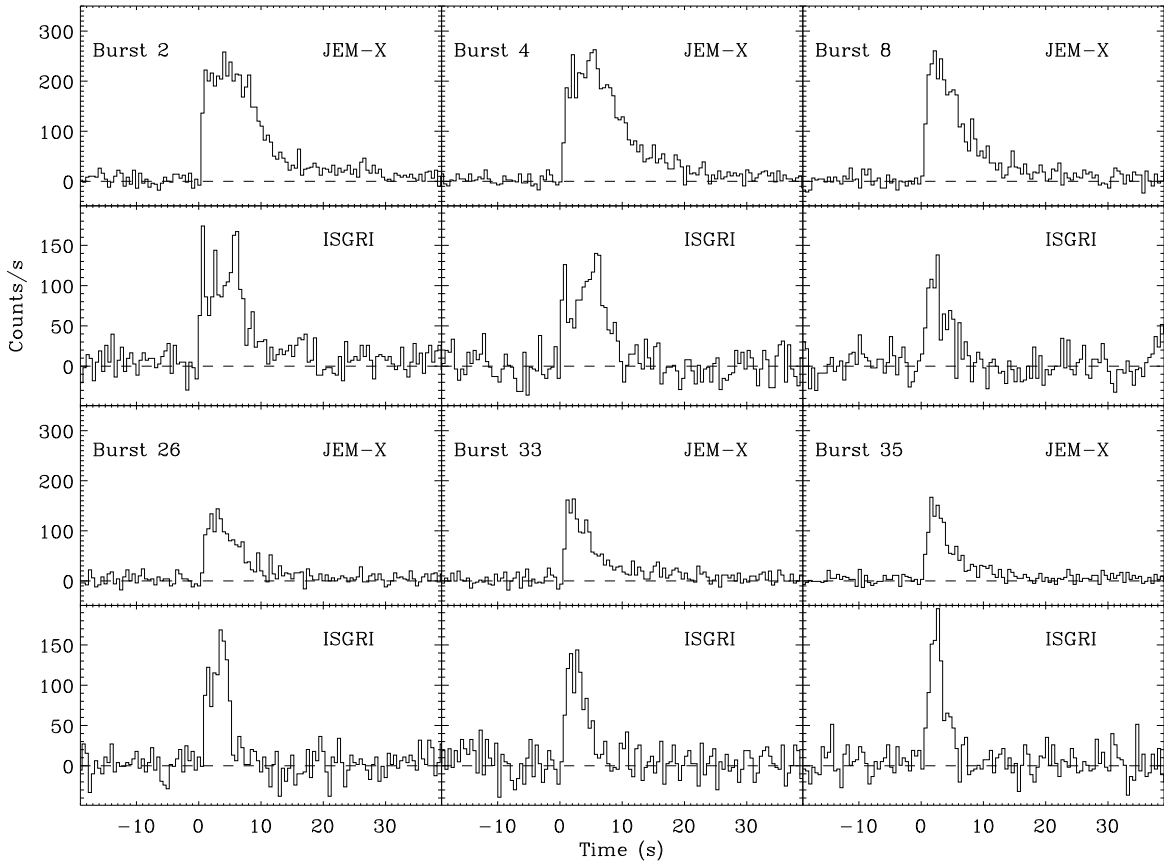


Fig. 2. Some examples of bright type I X-ray bursts detected from 4U 1728-34. For each burst the JEM-X (3–20 keV, upper panels) and IBIS/ISGRI (18–40 keV, lower panels) net light curves are shown (background subtracted). The time bin is 0.5 s for both IBIS/ISGRI and JEM-X. Bursts 2 and 4 show evidence of photospheric radius expansion.

3.2. Hardness Intensity Diagram of the persistent emission

To generate a CCD (see for this source e.g., Hasinger & van der Klis, 1989; Di Salvo et al., 2001; Franco, 2001) we used the background subtracted and burst subtracted JEM-X light curve with a 500 s time resolution. We defined the soft colour as the logarithm of the ratio of the count rate in the energy range 3–4.8 keV to the count rate in the range 4.8–7.7 keV. Similarly, we defined the hard colour in the range 7.7–12.5 keV and 12.5–20 keV. In this case the CCD was inadequate as the colour errors were as large as the colour variation. In order to reduce the errors on the colours, we generated a HID based on the net count rates in the 3–6 keV and 6–20 keV obtained in the single individual pointings of ~ 1800 s each. In our case the source behaviour is much better traced in the HID rather than in the CCD, because the statistical uncertainties are reduced along one of the two axes. The HID is shown in Fig. 3, with the positions superposed where the bursts were detected. Note that the patterns observed in a CCD are often also recognizable in the corresponding HID obtained by replacing soft colour by intensity, as applied e.g. on the Z sources GX 17+2

(Di Salvo et al., 2000; Farinelli et al., 2005), GX 5-1 (Muno, Remillard & Chakrabart, 2002) and on the atoll source Aql X-1 (Muno, Remillard & Chakrabart, 2002). This results from the intensity being dominated in the lower bands by soft photons whose thermal component correlates with temperature and therefore colour. The HID could indicate the banana branch of the atoll, with inferred accretion rate increasing along the atoll from left to right on the upper branch to the lower banana branch. To study the spectral variability of the source as a function of the HID position we divided the HID into nine regions, as shown in Fig. 3. The intervals were chosen in order to have good statistics for the spectral analysis. We averaged the different intensities with nearly the same hardness ratios and considering the nearness colours these spectra should be very similar. We also studied in more detail the 21 day long flare (see Fig. 1), divided among the boxes 6–9, represented by the filled dotted points in Fig. 3. The HID of the flare shows a transition from a hard to a soft state during 21 days with an intensity ratio $I_{\max}/I_{\min} \sim 10$ (see Sect. 4). This trend held also for the persistent emission, which also moved from a hard to soft state (boxes 1–5). This overall trend

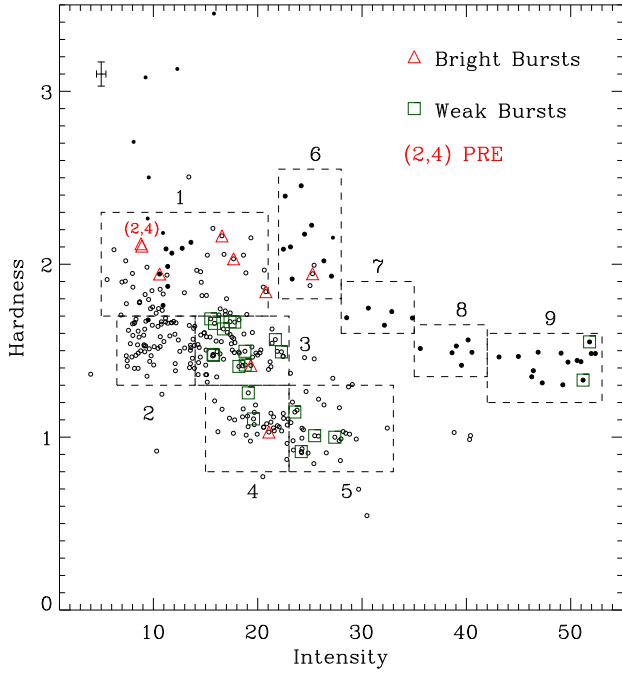


Fig. 3. HID of 4U 1728-34. The hardness is the ratio of the count rates in the 6–20 keV to 3–6 keV and the intensity is the 3–20 keV count rate. Each point (burst-subtracted) corresponds to ~ 1800 s of integration time. A typical error bar is shown at the top left corner. The boxes represent our selection of the data for the spectral analysis. The choice of the boxes (1–5 and 6–9) was made in order to study the spectral evolution along the atoll and to compare our result with previously studied 4U 1728-34 spectra. The filled dotted points are from the flare with $I_{\max}/I_{\min} \sim 10$ in the 3-20 keV energy band which lasted 21 days (see Fig. 1). The bursts detected with JEM-X and ISGRI are also indicated. Bursts 2 and 4 show evidence of a photospheric radius expansion episode.

can also be seen in the *RXTE*/ASM light curve (Fig. 7) for the period of this observation.

3.3. Spectral Analysis

The spectral analysis was done using XSPEC version 11.3 (Arnaud, 1996), combining the 20–200 keV ISGRI data with the simultaneous 5–20 keV JEM-X data. A constant factor was included in the fit to take into account the uncertainty in the cross-calibration of the instruments. The factor was fixed at 1 for the ISGRI data. A systematic error of 2% was applied to JEM-X/ISGRI spectra which corresponds to the current uncertainty in the response matrix. All uncertainties in the spectral parameters are given at a 90% confidence level for single parameters. For the source distance we use 4.5 kpc (Galloway et al., 2003, 2006).

3.3.1. Persistent emission variability

We studied the spectra of 4U 1728-34 along the atoll pattern for the different boxes reported in Fig. 3. A broad band 3–200 keV spectrum was obtained for each box using the joint JEM-X/ISGRI data and removing the time intervals corresponding to the bursts.

Atoll source spectra are successfully fitted by a two-component model consisting of a multicolour blackbody soft X-ray emission and a Comptonized spectrum, for the hard X-ray emission. The emission from the accretion shock on a neutron star is expected to be produced by thermal Comptonization of soft seed photons from the star, or from an optically thick boundary layer between accretion disc and NS surface (e.g., Zeldovich & Shakura, 1969; Alme & Wilson, 1973). We model the shock emission by the COMPTT model (Titarchuk, 1994) which is an analytic model describing Comptonization of soft photons in a hot plasma. We approximate the accretion shock geometry by a plane-parallel slab at the neutron star surface. The main model parameters are the Thomson optical depth across the slab, τ_T , the electron temperature, kT_e , and the seed photon temperature, kT_{seed} . The soft thermal emission, kT_{soft} , believed to be produced by the disc, is fitted by a multi-temperature disc model of (Mitsuda et al., 1984). We were not able to constrain the interstellar column density N_H (as the JEM-X bandpass starts above 3 keV), so we have set N_H to the value $2.5 \times 10^{22} \text{cm}^{-2}$ observed by *ROSAT* and *BeppoSAX*. We add to the fit a Gaussian line around 6.4 keV with a fixed width at $\sigma = 0.34$ keV as observed previously (e.g., Di Salvo et al., 2000; Piraino, Santangelo & Kaaret, 2000), but it was not statistically required. The multi-temperature disc model was also not required in the fit during the low/hard state. Soft emission (presumably from the accretion disc) during this state is difficult to detect since the JEM-X bandpass begins at 3 keV. Compton reflection between 10–30 keV was not required by the fit. The best fit parameters for each box are reported in Table 2 and in Fig. 5. For all the fits, the normalization constants of the JEM-X response were within 1.08 ± 0.09 . The nine unabsorbed νF_ν spectra and the residuals of the data to the model are shown in Fig. 4.

3.3.2. X-ray burst spectra

To study the net bursts' spectra, we first extracted the persistent emission spectrum excluding the outburst interval. We verified that during each burst pointing the count rate was stable, then we used the same fit models as described in Sect. 3.3.1 to fit the data. In Table 1 we report the mass accretion rate per unit area, \dot{m} , of the persistent emission for each burst pointing. This is given by $\dot{m} = \dot{M}/A_{\text{acc}}$, where A_{acc} is the area covered by $4\pi R_{\text{NS}}^2$. We assume a 10 km radius for the neutron star. The persistent mass accretion rate, \dot{M} , is calculated from $\dot{M} = L_{\text{pers}} \eta^{-1} c^{-2}$, where $\eta \sim 0.2$ is the accretion

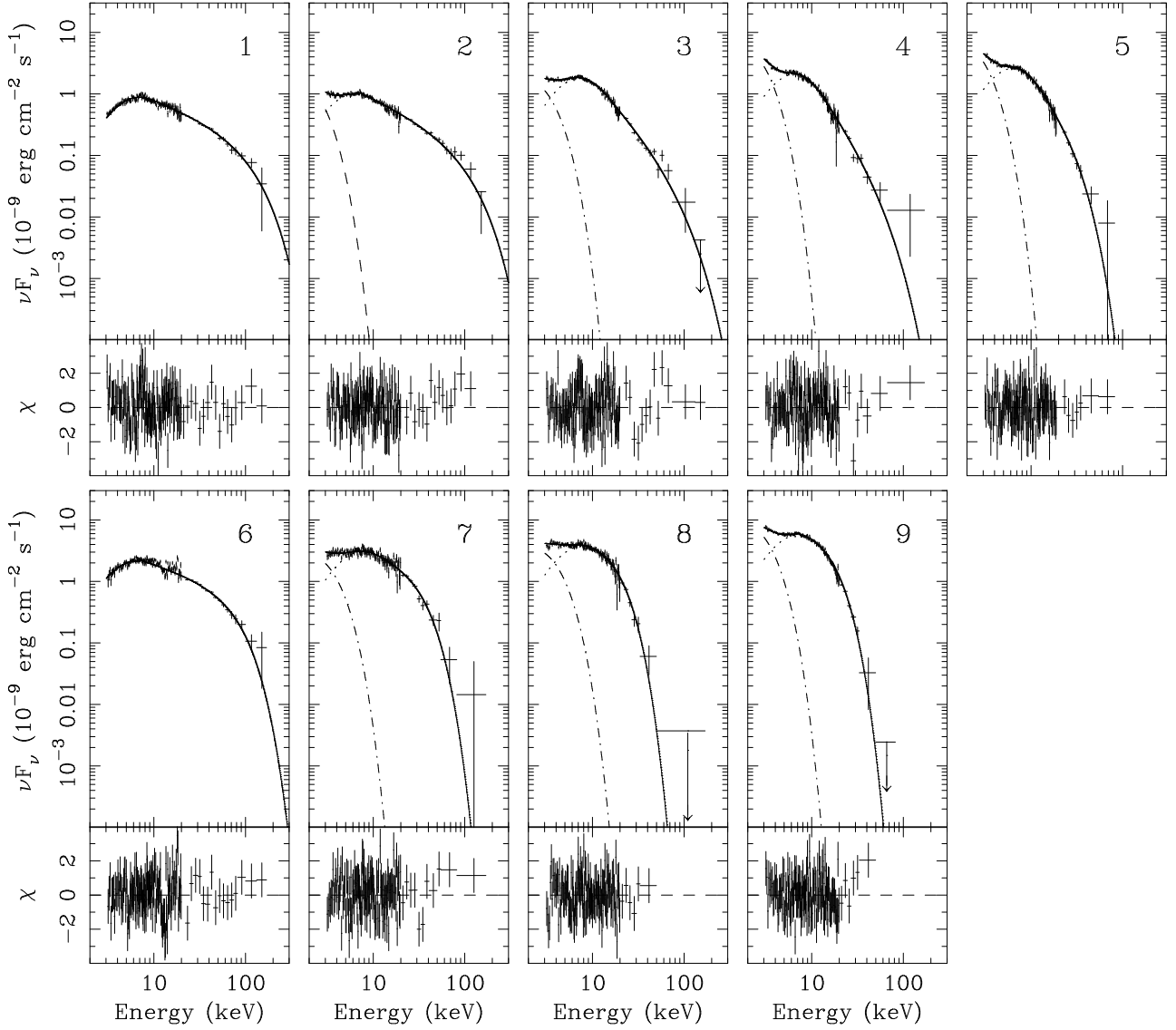


Fig. 4. *INTEGRAL*/JEM-X (3–20 keV) and ISGRI (20–200 keV) unfolded spectra of 4U 1728-34 along the “banana” track with the best fit DISKBB and COMPTT models. Residuals between the data and model are shown in the bottom panel in units of sigma. The spectra are labeled corresponding to each box number selected in the HID in Fig. 3. The best fit parameters are shown in Fig. 5 and Table 2.

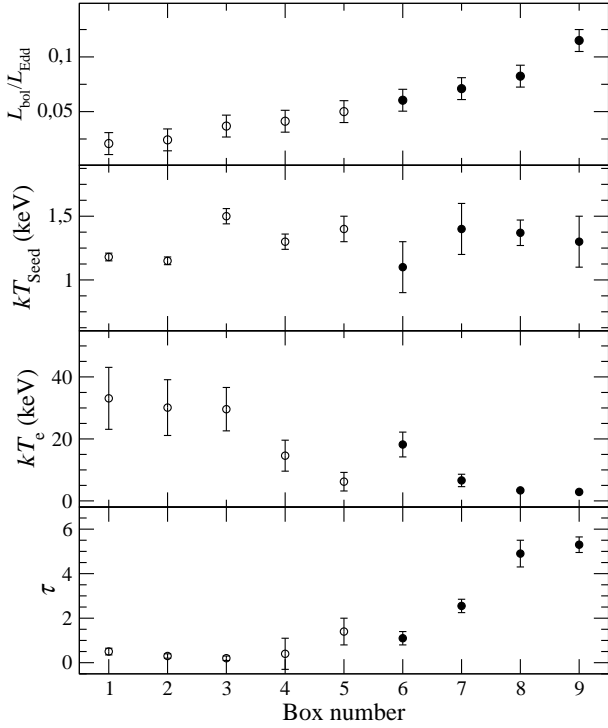
efficiency for a NS. The bursts occurred at a persistent emission level $L_{\text{pers}} \sim 2\text{--}8\% L_{\text{Edd}}$.

We then studied the net bursts’ time averaged spectra using for each burst the persistent emission spectra as background. The low statistics of JEM-X/ISGRI do not allow us to study the spectral evolution during the bursts. The spectra were extracted over the whole duration of each burst as determined from the JEM-X light curves. We also included in the fit the ISGRI spectra in the 18–40 keV energy bands. All obtained spectra were fitted by a photoelectrically absorbed blackbody. The unabsorbed flux between 0.1–200 keV, $F_{\text{bol,bb}}$, was calculated according to $F_{\text{bol,bb}} = 1.0763 \times 10^{-11} T_{\text{bb}}^{-4} K_{\text{bb}}^2 \text{ erg cm}^{-2} \text{ s}^{-1}$, where T_{bb} is the blackbody temperature in unit of keV and $K_{\text{bb}}(D, R_{\text{NS}})$ is the normalization of the blackbody component as returned by the fitting program. The black-

body temperature of the time averaged burst spectrum, kT_{bb} , was between 1.8 keV and 2.4 keV. The burst fluence, E_{b} , is calculated by integrating the measured $F_{\text{bol,bb}}$ over the burst duration. The burst peak flux, F_{peak} , was calculated by converting the peak count rate to flux using the averaged spectrum of each burst. Taking into account the typical blackbody temperature variation within the bursts (van Straaten, 2001), the associated error on our conversion factor is of the order of 12%, which is within our statistical errors. The best fit results and calculated burst parameters are reported in Table 1.

Table 2. Fit parameters of the persistent spectra in the energy range 3–200 keV

Parameter	Box 1	Box 2	Box 3	Box 4	Box 5	Box 6	Box 7	Box 8	Box 9
	(DISKBB + COMPTT)								
kT_{soft} (keV)	–	$0.54^{+0.3}_{-0.4}$	$0.7^{+0.3}_{-0.1}$	$0.6^{+0.5}_{-0.4}$	$0.6^{+0.3}_{-0.2}$	–	$0.73^{+0.23}_{-0.16}$	$0.78^{+0.12}_{-0.14}$	$0.65^{+0.15}_{-0.16}$
$N_{\text{soft}}^{1/2}$	–	40^{+12}_{-12}	20^{+5}_{-4}	62^{+15}_{-14}	58^{+11}_{-12}	–	30^{+9}_{-10}	27^{+8}_{-8}	69^{+17}_{-18}
kT_{seed} (keV)	$1.18^{+0.03}_{-0.03}$	$1.15^{+0.04}_{-0.03}$	$1.5^{+0.05}_{-0.07}$	$1.3^{+0.06}_{-0.06}$	$1.4^{+0.08}_{-0.2}$	$1.1^{+0.3}_{-0.2}$	$1.4^{+0.22}_{-0.16}$	$1.37^{+0.1}_{-0.14}$	$1.3^{+0.3}_{-0.13}$
kT_e (keV)	34.9^{+14}_{-6}	32.1^{+12}_{-7}	29.6^{+4}_{-10}	14.6^{+33}_{-7}	$6.2^{+4.7}_{-1.1}$	18.2^{+6}_{-2}	$6.6^{+1.2}_{-0.75}$	$3.4^{+0.29}_{-0.23}$	$2.9^{+0.12}_{-0.12}$
τ_T	$0.5^{+0.16}_{-0.2}$	$0.3^{+0.1}_{-0.1}$	$0.2^{+0.2}_{-0.07}$	$0.4^{+1.2}_{-0.3}$	$1.4^{+0.7}_{-0.5}$	$1.1^{+0.2}_{-0.6}$	$2.55^{+0.34}_{-0.4}$	$4.9^{+0.58}_{-0.56}$	$5.3^{+0.4}_{-0.3}$
χ^2/dof	146/133	144/144	150/139	149/134	123/131	160/134	160/136	129/130	126/133
$L_{3-200\text{keV}}^a$ (erg s ⁻¹)	3.8×10^{36}	4.4×10^{36}	6.7×10^{36}	7.5×10^{36}	9.1×10^{36}	1.1×10^{37}	1.3×10^{37}	1.5×10^{37}	2.1×10^{37}

^a Assuming a distance of 4.5 kpc. The DISKBB normalization is $N_{\text{soft}} \propto R_{\text{in}}^{1/2}$.**Fig. 5.** Spectral parameters from Table 2 as a function of the position on the HID.

4. Discussion

4.1. Origin of X-ray emission

We have fitted the 3–200 keV spectra of the atoll source 4U 1728-34 along its track on the HID by a two-component model: a thermal Comptonization model together with a soft component. The spectra and the parameters are shown in Fig. 4 and Fig. 5, respectively (see Table 2). The change in the spectral shape between the hard state (box/spectrum 1) and the soft state (box/spectrum 5) is clearly visible, as also during the flare (box/spectra 6–9), probably caused by a dramatic change in the accretion flow geometry. During the spectral evolution, spectra 1–5, at low intensity the optical depth was $\tau_T \sim 0.5$ with a high plasma temperature $kT_e \sim 35$ keV (box 1), and at higher intensity the optical depth was $\tau_T \sim 1.4$ with a

plasma temperature as low as $kT_e \sim 6$ keV (box 5). During this spectral change the luminosity increases from ~ 0.02 to $0.05 L_{\text{Edd}}$, where the seed photons temperature was almost constant at $kT_{\text{seed}} \sim 1.3$ keV. The same behaviour is observed also during the flare event (box 6–9) where the plasma temperature decreases from ~ 18 to 3 keV and the optical depth increases from 1 to 5 and the spectral change the luminosity increases from ~ 0.06 to $0.12 L_{\text{Edd}}$. We observe a typical atoll spectral change from a low or intermediate/hard state to a high/soft state, where the accretion rate increases from the hard state to the soft state. The soft component could be associated with the radiation from the accretion disc.

With our coverage of luminosity variation, $F_{\text{max}}/F_{\text{min}} \approx 2.5$, observed during ~ 7.4 days integration time between 2003 February and 2004 October we are probably not observing the full atoll track, even during the flare (see Fig. 3). We observe the source most likely from a intermediate/hard state, upper banana, to the soft state, lower banana state, and probably not during the island state. If the source was in the island state, we could also expect that more than two bursts with PRE are observed (see Sect. 4.2). The hard component observed during the hard/intermediate state is explained with Comptonization of seed photons from a NS surface by hot electrons in an inner optically thin accretion flow (or outer boundary layer). The optically thin Comptonization medium has temperature of ≥ 20 keV. The observed plasma temperature and optical depth during the spectra 1–3 are typically hard/intermediate state parameters, only during the flare we observe typically lower banana state parameters. In the lower banana branch spectra the Comptonized component is much softer, with temperature of ~ 6 keV and optical depth of $\gg 1$ as observed during the spectra 5–9.

From our fits it results that the hard spectra can be described by unsaturated Comptonization of soft photons in the hot $kT_e \sim 20 - 30$ keV optically thin $\tau \sim 0.5 - 1$ plasma. However, different models have been proposed to explain the different emission region and emission mechanism during the different spectral states and evo-

lution (Mitsuda et al., 1989; Zeldovich & Shakura, 1969; Alme & Wilson, 1973; White, Stella & Parmer, 1988).

If the soft photons are emitted from a disc, then the inner disc radius can be estimated from the DISKBB model as

$$R_{\text{in}} \approx 0.76 N_{\text{soft}}^{1/2} \frac{2.7}{\eta} \frac{4.5}{D} \left(\frac{f_{\text{col}}}{1.8} \right)^2 \left(\frac{0.5}{\cos i} \right)^{1/2} \text{ km}, \quad (1)$$

where D is the source distance, i is the inclination angle of the system, f_{col} is the ratio of the colour to effective temperature (Shimura & Takahara, 1995) and η is the correction factor for the inner torque-free boundary condition (Gierliński et al., 1999, $\eta = 2.7$ for $R_{\text{in}} \sim R_{\text{NS}}$ and less for higher R_{in}). With $D = 4.5$ kpc, $f_{\text{col}} = 1.8$ and using a mean inclination angle of $i = 60^\circ$ we find $R_{\text{in}} = 15 \pm 3 \div 52 \pm 13$ km. For 4U 1728-34 the observed QPO are related on their position in the CCD/HID (Méndez & van der Klis, 1999; Di Salvo et al., 2001; Migliari, van der Klis, & Fender, 2003). Among the most frequently used QPO models, the upper kHz QPO is related to the Kepler frequency, i.e. $\nu_{\text{QPO}} = \nu_{\text{Kepler}} \approx 1184 \text{ Hz} (R_{\text{in}}/15 \text{ km})^{-3/2} M_{\odot,1.4}^{1/2}$, at the innermost stable orbit of the accretion disc (for a review see van der Klis, 2004, and reference therein). Using our measured inner disc radius, R_{in} , the upper kHz QPO has to be in the frequency range from 1160 ± 300 Hz to 213 ± 53 Hz. These values are consistent with the upper kHz QPO values of 4U 1728-34 (Di Salvo et al., 2001). However, using this relation we are not able to exactly locate the source position in the CCD/HID.

We have measured the plasma temperature, optical depth, and flux of 4U 1728-34 over a range of positions on the HID for the first time. We compare with previously reported time averaged spectra (Grindlay & Hertz, 1981; Basinska et al., 1984; White et al., 1986; Claret et al., 1994; Schulz, 1999; Di Salvo et al., 2000; Piraino, Santangelo & Kaaret, 2000; Narita, Grindlay & Barret, 2001; D’Ai et al., 2006). Accounting for the fact that these authors have reported time averaged spectra sometimes over possibly different spectral states, and sometimes only in energy ranges less than 20 keV, and insofar as the models used to fit the data are consistent, we found that all the previous reported spectral parameters are consistent with our measurements. For example, Claret et al. (1994), using *SIGMA* (30-200 keV) data, measured plasma temperatures kT_e of ~ 5 and ~ 30 keV in two different source states. These correspond to our reported soft and hard states. Also using a broad band spectrum, BeppoSAX observed the source with $kT_e \sim 7$ keV and $\tau \sim 5$, also consistent with an intermediate soft state. We would like to point out, in order to determine the source states with more confidence, how important it is for 4U 1728-34 to have: (i) a high energy spectrum above 20 keV, and (ii) not to average the spectra over a long time period. (i) using the JEM-X and ISGRI broad band spectrum (box 1) from 3–200 keV, in the intermediate/hard state,

the thermal Comptonization plasma temperature was ~ 35 keV, considerably higher than the value (~ 10 keV) derived from the low energy 3–20 keV JEM-X data alone. (ii) a flux variation of a factor 1.12 will already change the spectral parameters and a factor 2 will drastically change the source state (see Table 2). Note also, e.g., that during the flare we have $I_{\text{max}}/I_{\text{min}} \sim 10$ in the 3–20 keV band which corresponds to a flux variation of $F_{\text{max}}/F_{\text{min}} \sim 2$ in the 3–200 keV band. This shows again for 4U 1728-34 how important the energy contribution is above 20 keV.

4.2. Type I X-ray bursts

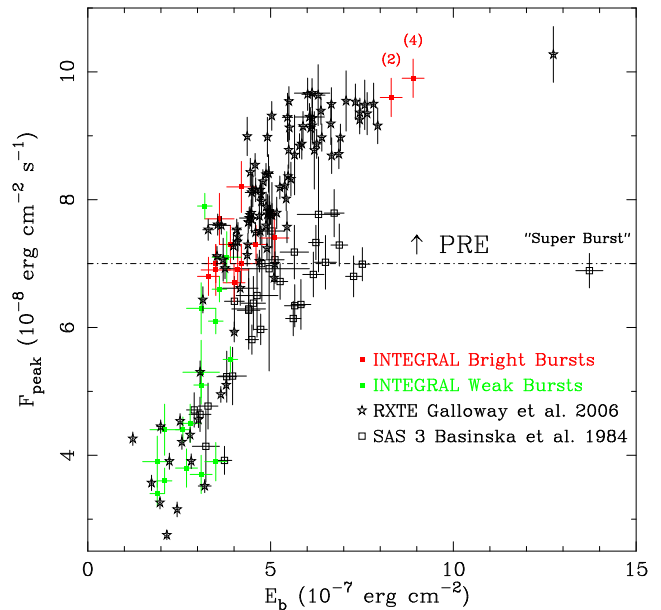


Fig. 6. Relation between peak flux, F_{peak} , and burst fluence, E_b . The dashed line indicates the lower limit of the observed photospheric radius expansion events. The two *INTEGRAL* bursts exhibiting PRE are labeled with the number 2 and 4 as reported in Table 1.

More than 200 bursts have been observed in 4U 1728-34 since its discovery (Hoffman et al., 1976; White et al., 1986; Basinska et al., 1984; Foster, Ross, & Fabian, 1986; Day & Tawara, 1990; Franco, 2001; van Straaten, 2001; Galloway et al., 2003, 2006). Compared to the previously observed bursts, ours appear as ordinary bursts observed for this source. All the detected bursts have a rise time about 1 s with a e-fold decay time from 3–7 s in the 3–20 keV energy band. Most of the bursts are observed up to 30–40 keV during the first 5–10 s, and the energetic ones are observed at the lowest inferred mass accretion rate (see Fig. 3). Such behaviour was observed e.g., also for GX 3+1, where a super burst and a unusually long burst occurred at the lowest mass accretion rate (Kuulkers & van der Klis, 2000; Chenevez et al., 2006).

The averaged spectrum during the burst measured a blackbody temperatures from 1.8 to 2.4 keV with a bolometric flux from 1.7×10^{-8} to 4.5×10^{-8} erg cm $^{-2}$ s $^{-1}$, respectively. This corresponds to an effective emission radius (i.e., $R_{\text{eff}} = d_{10\text{kpc}} F_{\text{bol}}^{1/2} T_{\text{bb}}^{-2} \sigma^{-1/2} (z+1)^{-1/2}$ where $z+1 = 1.31$ is the gravitational redshift correction and σ is the Stefan-Boltzman constant), R_{eff} , from $\sim 4.5 d_{4.5\text{kpc}} \div 3.8 d_{4.5\text{kpc}}$ km, assuming a NS radius of 10 km, a NS mass of $1.4 M_{\odot}$ and isotropic emission. This emission radius could be attributed to an extended part of the NS surface.

In Fig. 6 we show the bursts’ peak flux, F_{peak} , plotted as a function of the integrated burst flux, E_{b} , including the 32 and 104 bursts observed by *SAS 3* and *RXTE* (Basinska et al., 1984; Galloway et al., 2006). Note that a subset of the *RXTE* bursts were reported and discussed in (Galloway et al., 2003). Most of the bursts with a higher peak flux as $\sim 7 \times 10^{-8}$ erg cm $^{-2}$ s $^{-1}$ show double-peaked behaviour, these energy-dependent double-peaked profile are also the result of PRE. All the bursts below the dashed line are bursts without PRE. The *INTEGRAL* bursts, excluding bursts with PRE, occurred at a persistent emission flux minimum and maximum level of $\sim 2.2 \times 10^{-9}$ and $\sim 8.8 \times 10^{-9}$ erg cm $^{-2}$ s $^{-1}$ ($\dot{m} \sim 2.4 \times 10^3 \div 9.4 \times 10^3$ g cm $^{-2}$ s $^{-1}$), respectively (3–20 keV). The values without PRE observed by *SAS 3* (Basinska et al., 1984) are within the *INTEGRAL* observation. The averaged value of the persistent emission during the *SAS 3* observation was $\sim 3.25 \times 10^{-9}$ erg cm $^{-2}$ s $^{-1}$ (1–20 keV) and varied by a factor ~ 1.25 . The *INTEGRAL* bursts with PRE, burst 2 and 4, occurred at the lowest mass accretion rate of $\sim 1.7 \times 10^3$ g cm $^{-2}$ s $^{-1}$. The bursts total fluence, and the bursts peak flux are anti-correlated with the mass accretion rate. From a 30 days averaged *RXTE*/*ASM* light curve (1.5–12 keV) (Levine et al., 1996) the persistent flux of 4U 1728-34 shows a variation of about a factor three on a ~ 7.7 yr time scale and *INTEGRAL* observed 4U 1728-34 during a bright persistent emission phase (see Fig. 7). Indeed the only two bursts with PRE were observed at the the lowest mass accretion rate at the start of the *INTEGRAL* observation, all other bursts without PRE are observed at higher mass accretion rate.

The lowest inferred mass accretion rate at the $\sim 7 \times 10^{-8}$ erg cm $^{-2}$ s $^{-1}$ line (see Fig. 6) is $\dot{m} \approx 2.4 \times 10^3$ g cm $^{-2}$ s $^{-1}$. From the observed burst properties (see Table 1) and inferred mass accretion rates, the present theory predicts that these bursts are pure helium burning (e.g. Strohmayer & Bildsten, 2004). For helium flashes, the fuel burns rapidly, since there are no slow weak interactions, and the local Eddington limit is often exceeded. These conditions lead to PRE bursts with a duration, set mostly by the time it takes the heat to escape, of the order of 5–10 s, as observed. The *INTEGRAL*-observed bursts without PRE with a mass accretion rate of $\gtrsim 2.4 \times 10^3$ g cm $^{-2}$ s $^{-1}$ could also arise from helium burning. In the framework of the thermonuclear-flash models (e.g., Lewin, van Paradjis, & Taam, 1995) the burst duration,

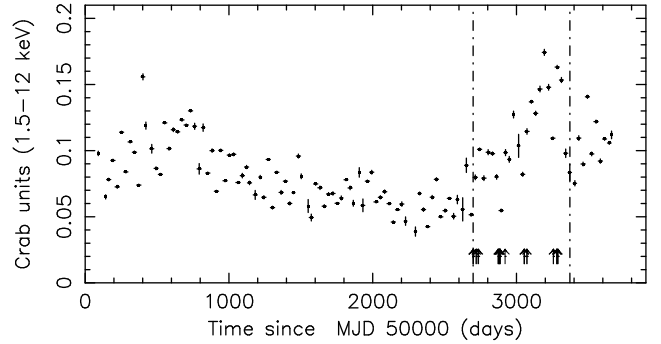


Fig. 7. 30-day averaged *RXTE*/*ASM* light curve in the 1.5–12 keV energy band showing the long term variability of 4U 1728-34 from 1996 to 2005. The vertical dashed lines indicate the time interval of the *INTEGRAL* observations. The *ASM* count rates has been converted into flux using 1 Crab Unit for 75 cts/s. The arrows indicate the time of the type I bursts.

$\tau = E_{\text{b}}/F_{\text{peak}} < 10$ s, and the ratio of the observed persistent flux to the net peak flux, $\gamma = F_{\text{pers}}/F_{\text{peak}}$, indicate a hydrogen-poor burst, i.e., pure helium bursts. We found a good agreement with the predicted amount of liberated helium fuel during the bursts with the observed accreted mass between two bursts (calculated only for the bursts with known α parameter). The amount of fuel liberated in the thermonuclear burning is calculated as $L_{\text{b}}/\epsilon_{\text{He}}$, where L_{b} is the observed burst total fluence and $\epsilon_{\text{He}} \approx 1.7$ Mev/nucleon $\approx 1.6 \times 10^{18}$ erg g $^{-1}$ is the He energy release. For instance, for burst 2, $\Delta M = \dot{M}\Delta t \sim 1.2 \times 10^{21}$ g is in agreement with the predicted amount of liberated helium fuel during this burst $L_{\text{b}}/\epsilon_{\text{He}} \sim 1.3 \times 10^{21}$ g. We observed pure helium bursts during the different spectral states. 4U 1728-34 shows the same burst properties as the ultracompact 10 minute binary 4U 1820-30 (Cumming, 2003). In Fig. 6 we also show the so-called “super burst” by Basinska et al. (1984). Super bursts, as currently understood and observed, have a duration of several hours, a total fluence of $\sim 10^{42}$ erg and are believed to be due to unstable burning of a thick carbon layer (e.g. Strohmayer & Bildsten, 2004). The observed “super burst” by Basinska et al. (1984) was most likely also a helium burst with PRE triggered after a longer burst recurrence time.

5. Summary

We analyzed the spectral and bursting behaviour from the simultaneous *INTEGRAL* IBIS/ISGRI and JEM-X observation of 4U 1728-34, which was spatially well distinguished from the neighbouring source, the Rapid Burster. The broad band spectra from 3–200 keV is well described by a thermal Comptonization model with seed photons from the neutron star surface scattered in a shock-heated accretion column above the hot spot region, or from an optically thick boundary layer between accretion disc and NS surface. The thermal blackbody soft emission could arise

from the accretion disc. The spectral evolution observed from an intermediate/hard state to the soft state are entirely typical of atoll sources. With increasing mass accretion rate the source spectra become brighter and softer. We observed a decreasing electron temperature from 35–3 keV an increase of the optical depth from 0.5–5, during the source luminosity increase from 2-12% of Eddington, i.e. from the intermediate/hard state to the soft state.

The 36 type I bursts show an anti-correlation between burst peak flux or fluence with the mass accretion rate. At low mass accretion rate, intermediate/hard state, most of the bursts show PRE with a peak flux exceeding the Eddington luminosity, at higher mass accretion rate, soft state, the bursts were normal type I bursts. We observed normal X-ray bursts for this source involving pure helium either during PRE in the intermediate/hard state, or during the soft state.

Acknowledgements. MF and DG acknowledge the French Space Agency (CNES) for financial support. MF is grateful to D. Galloway for providing us with the *RXTE* data used in Figure 6 and for valuable discussions. The data reported in this paper are based on observations with *INTEGRAL*, an ESA project with instruments and the science data center funded by ESA member states (especially the PI countries: Denmark, France, Germany, Italy, Switzerland, Spain), Czech Republic and Poland, and with the participation of Russia and the USA. ISGRI has been realized and maintained in flight by CEA-Saclay/DAPNIA with the support of CNES.

References

- Alme, M. L., & Wilson, J. R. 1973, *ApJ*, 186, 1015
- Arnaud, K. A. 1996, in *Astronomical Data Analysis Software and Systems V*. ed. G. H. Jacoby, & J. Barnes, ASP Conf. Series 101 (San Francisco: ASP), 17
- Barret, D. 2001, *AdSpR*, 28, 307
- Basinska, E. M., Lewin, W. H., Sztajno, M., Cominsky, L. R., Marshall, F. J. 1984, *ApJ*, 281, 337
- Cumming, A. 2003, *ApJ*, 595, 1077
- Chenevez, J., Falanga, M., Brandt, S. 2006, *A&A*, 449, L5
- Chakrabarty, D., Morgan, E. H., Munro, M. P., et al. 2003, *Nature*, 424, 42
- Claret, A., Goldwurm, A., Cordier, B., et al. 1994, *ApJ*, 423, 436
- Cornelisse, R., in't Zand, J. J. M., Verbunt, F., et al. 2003, *A&A*, 405, 1033
- Courvoisier, T. J.-L., Walter, R., Beckmann, V., et al. 2003, *A&A*, 411, L57
- D'Ài, A., Di Salvo, T., Iaria, et al. 2006, *A&A*, 448, 817
- Day, C. S. R., & Tawara, Y. 1990, *MNRAS*, 245, 31
- Di Salvo, T., Iaria, R., Burderi, L., Robba, N. R. 2000, *ApJ*, 542, 1034
- Di Salvo, T., Stella, L., Robba, N. R., et al. 2000, *ApJ*, 544, L199
- Di Salvo, T., Méndez, M., van der Klis, M., et al. 2001, *ApJ*, 546, 1007
- Falanga, M., Farinelli, R., Goldoni, P., et al. 2004, *A&A*, 426, 979
- Farinelli, R., Frontera, F., Zdziarski, A. A., et al. 2005, *A&A*, 434, 25
- Forman, W., Tananbaum, H. & Jones, C. 1976, *ApJ*, 206, L29
- Foster, A., J, Ross, R. R., & Fabian, A. C. 1986, *MNRAS*, 221, 409
- Franco, L. M., 2001, *ApJ*, 554, 340
- Galloway, D. K., Psaltis, D., Chakrabarty, D., Munro, M. P. 2003, *ApJ*, 590, 999
- Galloway, D. K., et al. 2006, in preparation
- Goldwurm, A., Daid, P., Foschini, L., et al. 2003, *A&A*, 411, L223
- Gros, A., Goldwurm, A., Cadolle-Bel, M., et al. 2003, *A&A*, 411, L179
- Gierliński, M., Zdziarski, A. A., Poutanen, J., et al. 1999, *MNRAS*, 309, 496
- Gierliński, M., Done, C. 2002, *MNRAS*, 337, 1373
- Grindlay, J. E., & Hertz, P. 1981, *ApJ*, 247, L17
- Hoffman, J. A., Lewin, W. H. G., Doty, J., et al. 1976, *ApJ*, 210, L13
- Hasinger, G., & van der Klis, M. 1989, *A&A*, 225, 79
- Lebrun, F., Leray, J.-P., Lavocate, Ph., et al. 2003, *A&A*, 411, L141
- Levine, A. M., Bradt, H., Cui, W. 1996, *ApJ*, 469, L33
- W. H. G. Lewin, J., van Paradjis, & R. E., Taam, in *X-ray Binaries*, eds. W. H. G. Lewin, J., van Paradjis, & E. P., J., van den Heuvel, 1995, (Cambridge Univ. Press)
- Lewin, W. H. G., van Paradjis, J., & Taam, R. 1993, *Space Sci. Rev.*, 62, 223
- W. H. G. Lewin, & P. C. Joss, in *Accretion-Driven Stellar X-ray Sources*, eds. W. H. G. Lewin & E. P., J., van den Heuvel, 1983, (Cambridge Univ. Press)
- Lund, N., Budtz-Joergensen, C., Westgaard, N. J., et al. 2003, *A&A*, 411, L231
- Mereghetti, S., Götz, D., Borkowski, R., et al. 2003, *A&A*, 411, L291
- Méndez, M., & van der Klis, M. 1999, *ApJ*, 517, L51
- Migliari, S., van der Klis, M., & Fender, R. P. 2003, *MNRAS*, 345, L35
- Mitsuda, K. K., Inoue, H., Koyama, K., et al. 1984, *PASJ*, 36, 741
- Mitsuda, K., Inoue, H., Nakamura, N., Tanaka, Y., et al. 1989, *PASJ*, 41, 97
- Munro, M. P., Remillard, R., A., Chakrabarty, D., 2002, *ApJ*, 568, L35
- Narita, T., Grindlay, J. E., & Barret, D. 2001, *ApJ*, 547, 420
- Piraino, S., Santangelo, A., & Kaaret, P. 2000, *A&A*, 360, L35
- Psaltis, D., Belloni, T., van der Klis, M. 1999, *ApJ*, 520, 262
- Kuulkers, E. & van der Klis, M. 2000, *A&A*, 356, L45
- Poutanen, J., & Svensson, R. 1996, *ApJ*, 470, 249
- Schulz, N. S. 1999, *ApJ*, 511, 304
- Shimura, T., & Takahara, F. 1999, *ApJ*, 445, 780
- Strohmayer, T. E., Zhang, W., Swank, K. H., et al. 1996, *ApJ*, 469, L9
- Strohmayer, T. E., Markwardt, C. B., 1999, *ApJ*, 516, L81
- Strohmayer, T. E., & Bildsten, L. 2004, in *Compact stellar X-ray sources*, ed. W. H. G. Lewin & M. van der Klis, (Cambridge: Cambridge University Press), [arXiv:astro-ph/0301544]
- Titarchuk, L. 1994, *ApJ*, 434, 570
- Ubertini, P., Lebrun, F., Di Cocco, G., et al. 2003, *A&A*, 411, L131
- van der Klis, M., 2004, in *Compact stellar X-ray sources*, ed. W. H. G. Lewin & M. van der Klis, (Cambridge: Cambridge University Press), [arXiv:astro-ph/0410551]

- van Straaten, S., van der Klis, M., Kuulkers, E., & Méndez, M. 2001, *ApJ*, 551, 907
- Verbunt, F., & van den Heuvel, E. P. J. 1995, in *X-ray binaries*, ed. W. H. G. Lewin, J. van Paradijs, & E. P. J. van den Heuvel (Cambridge: Cambridge University Press), 457
- Wijnands, R., & van der Klis, M. 1999, *A&A*, 514, 939
- Winkler, C., Courvoisier, T. J.-L., Di Cocco, G., et al. 2003, *A&A*, 411, L1
- White, N. E., Stella, L., & Parmar, A. N. 1988, *ApJ*, 324, 363
- White, N. E., Peacock, A., Hasinger, G., et al. 1986, *MNRAS*, 218, 129
- Zel'dovich, Ya. B., & Shakura, N. I. 1969, *Sov. Astron.*, 13, 175